Supplementary Information for

"Resonant Tunneling induced large magnetoresistance in vertical van der Waals magnetic tunneling junctions based on type-II spin gapless semiconductor VSi_2P_4"

Jiangchao Han,[a,b†] Daming Zhou,[b†] Wei Yang,[b] Chen Lv,[b] Xinhe Wang,[b] Guodong Wei,[b] Weisheng Zhao,[b] Xiaoyang Lin[c*] and Shengbo Sang[a*]

[a]College of Electronic Information and Optical Engineering, Taiyuan University of Technology, Taiyuan 030024, China

[b]Fert Beijing Institute, MIIT Key Laboratory of Spintronics, School of Integrated Circuit Science and Engineering, Beihang University, Beijing 100191, China

[c]National Key Lab of Spintronics, Institute of International Innovation, Beihang University, Yuhang District, Hangzhou, 311115, China

[†]These authors contributed equally to this work.

[*]E-mail: XYLin@buaa.edu.cn; sangshengbo@tyut.edu.cn

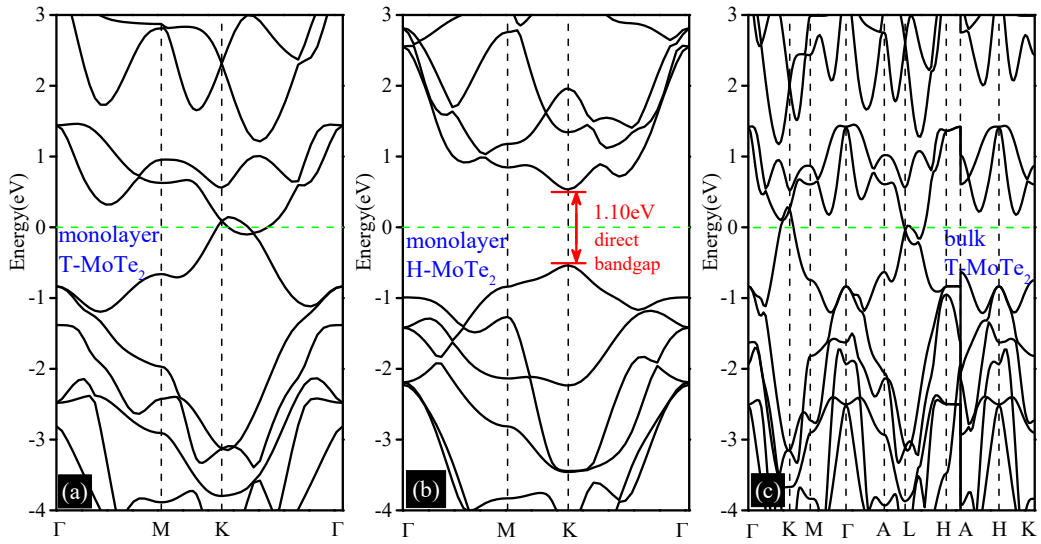

Fig. S1 The band structures of monolayer T-$MoTe_2$, monolayer H-$MoTe_2$ and bulk T-$MoTe_2$.

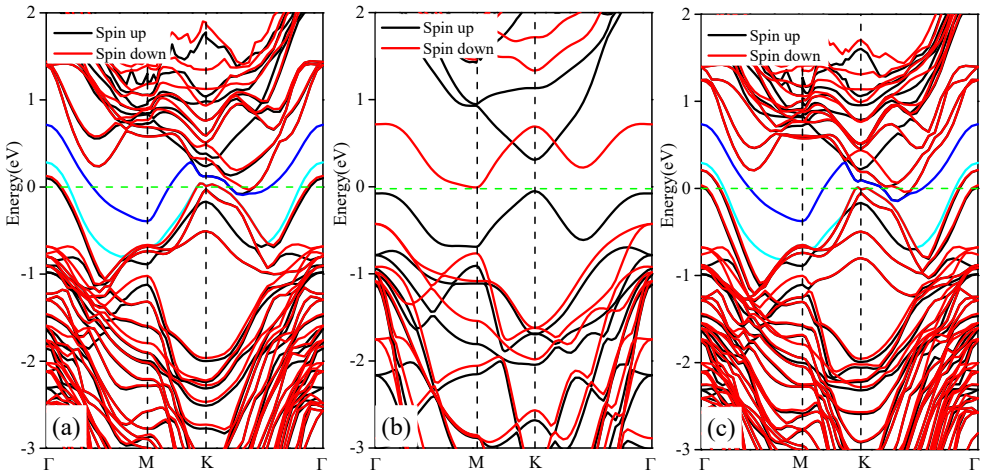

Fig. S2 Spin-dependent band structures of (a) 1H heterostructure, (b) monolayer VSi_2P_4 and (c) 3H heterostructure. Cyan (blue) line represents the corresponding VBM (CBM) in spin up (spin down) channel for monolayer VSi_2P_4.

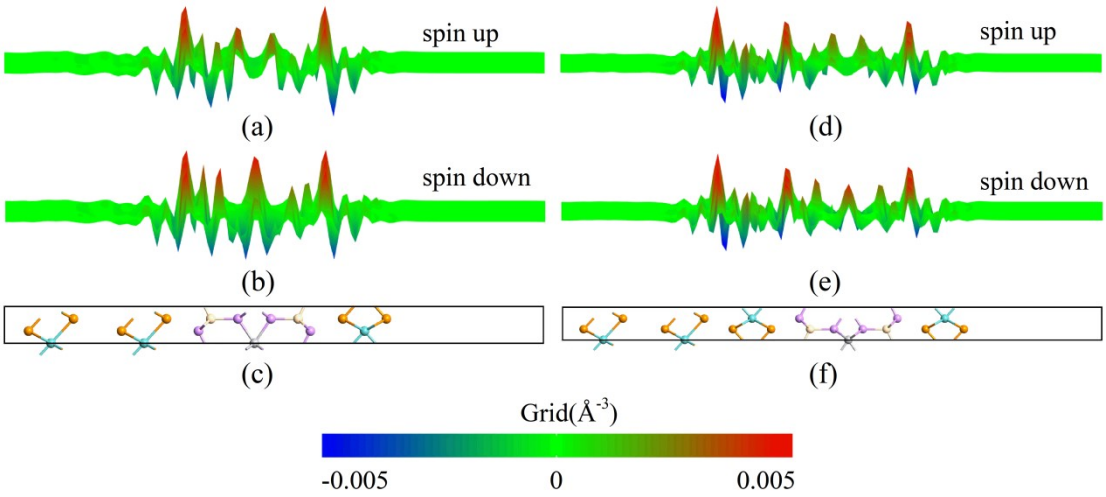

Fig. S3 The differential charge densities [(a), (b), (d) and (e)] and the corresponding heterostructures [(c) for 1H device and (f) for 3H device]. The red and blue colors represent the charge accumulation and depletion regions, respectively.

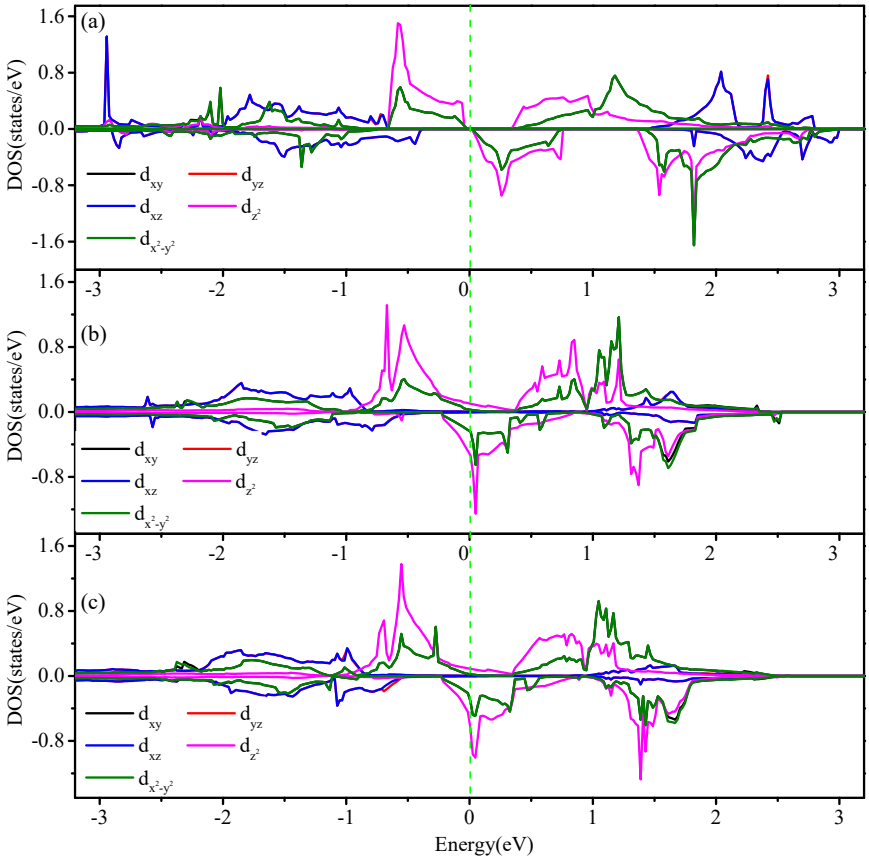

Fig. S4 The projected orbitals' density of states (DOS) for V in (a) monolayer VSi_2P_4, (b) 1H heterostructure and (c) 3H heterostructure.

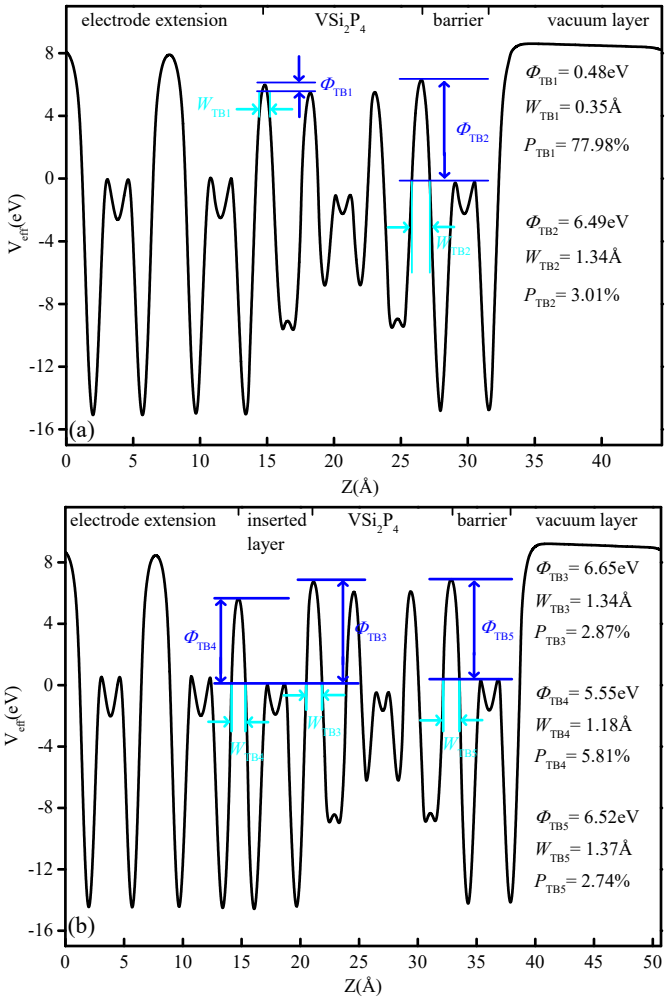

Fig. S5 The electrostatic potential profiles along the transport direction for 1H heterostructure (a) and 3H heterostructure (b).

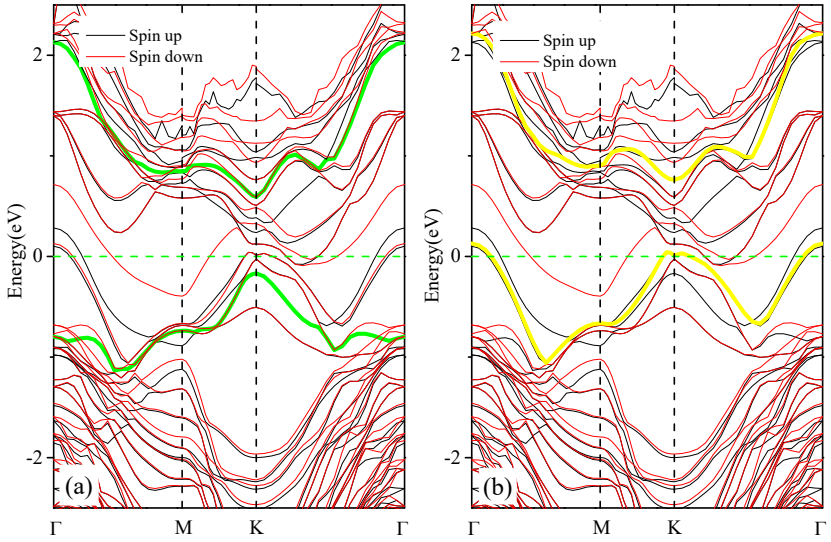

Fig. S6 The spin-dependent band structures of 1H heterostructure. The green lines (yellow lines) show the VBM and CBM of middle H-$MoTe_2$ in spin up (spin down) channel.

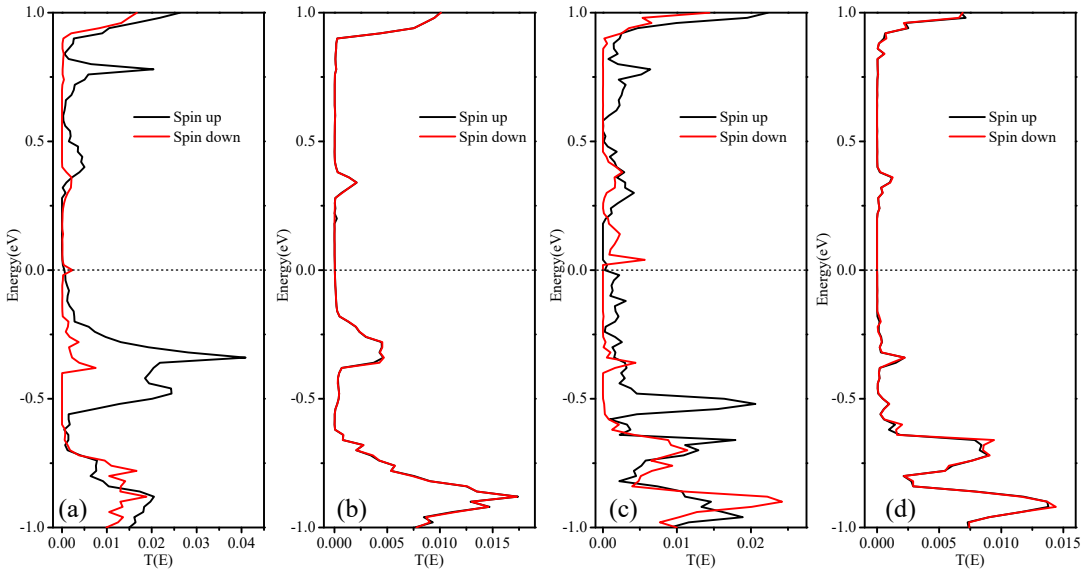

Fig. S7 The spin-dependent transport spectrums of 1H [(a) and (b)] and 3H [(c) and (d)] heterostructures. (a) and (b) for PC, (c) and (d) for APC.

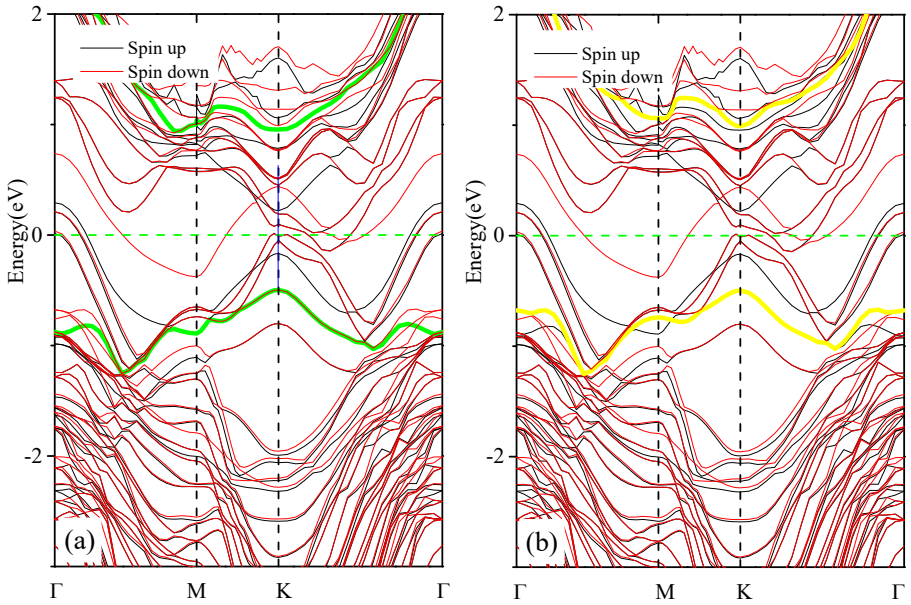

Fig. S8 The spin-dependent band structures of 3H heterostructure. The green lines (yellow lines) show the VBM and CBM of middle H-$MoTe_2$ in spin up (spin down) channel.

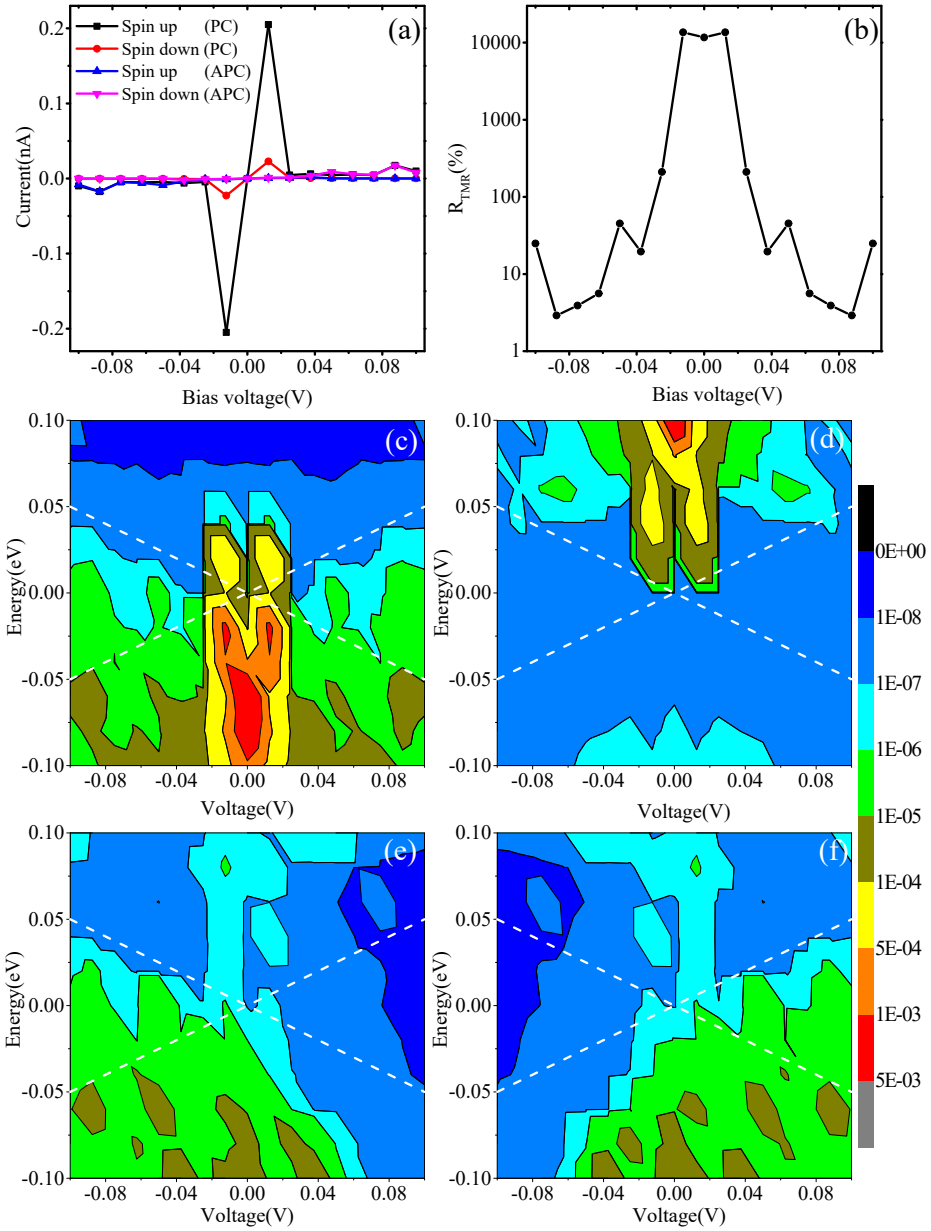

Fig. S9 (a) The bias-voltage-driven spin-dependent currents of 3H device and the TMR with the change of bias voltage (b). The spin-dependent transmission spectra of 3H device in the PC [(c) and (d)] and the APC [(e) and (f)], (c) and (e) for spin up channels, (d) and (f) for spin down channels.

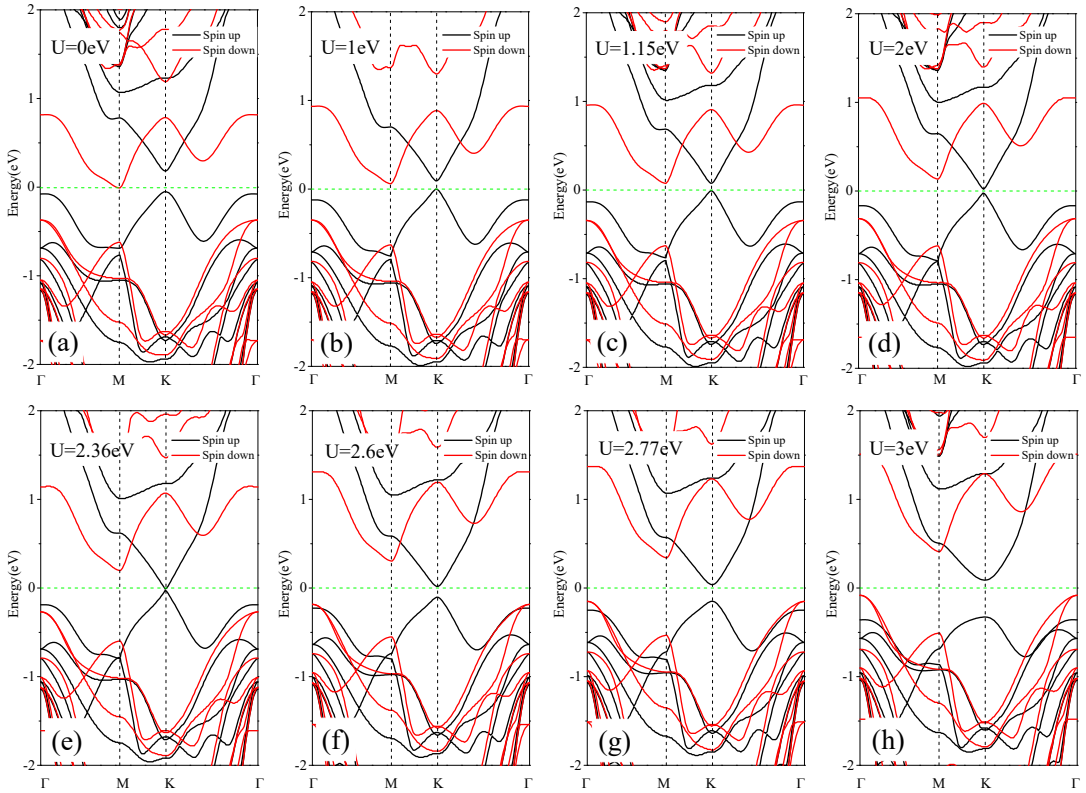

Fig. S10 Spin-polarized band structures of monolayer VSi_2P_4 obtained from GGA+U without SOC.

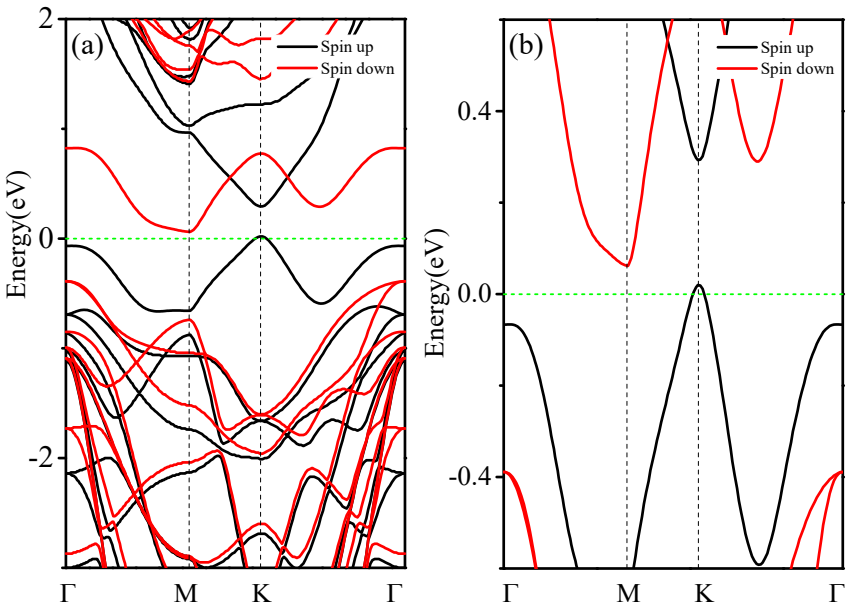

Fig. S11 The spin-dependent bandstructures of monolayer VSi_2P_4 including using advanced pseudopotential.

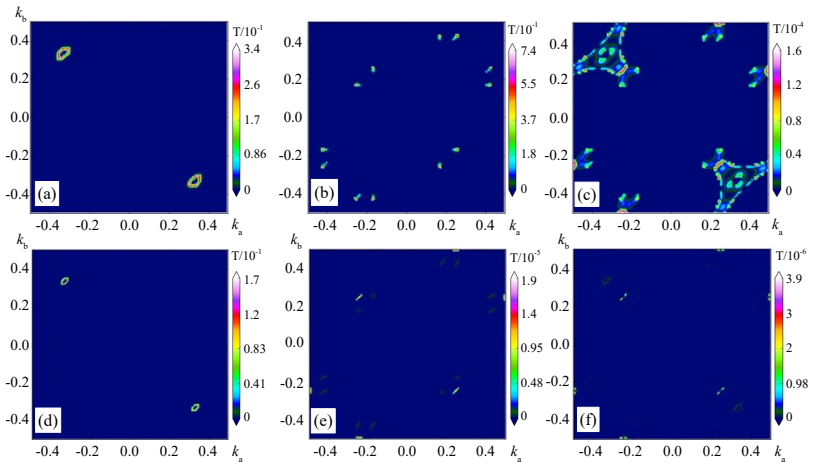

Fig. S12 The spin-resolved transmission coefficients for 1H [(a)-(c)] and 3H [(d)-(f)] devices including using advanced pseudopotential. [(a) and (d)]/[(b) and (e)] are for the spin up/down channel of PC, [(c) and (f)] are for spin up channel of APC.

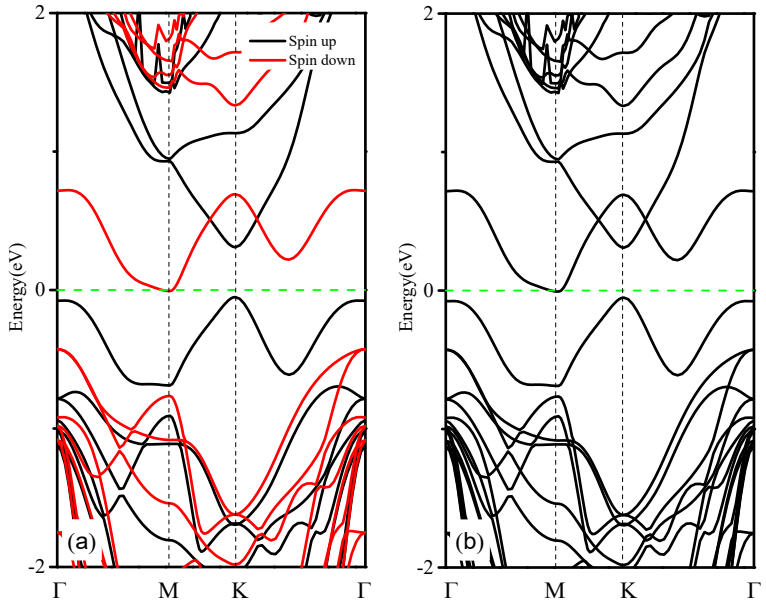

Fig. S13 The spin-dependent band structures of monolayer VSi_2P_4 including using GGA (a) or GGA+SOC (b).

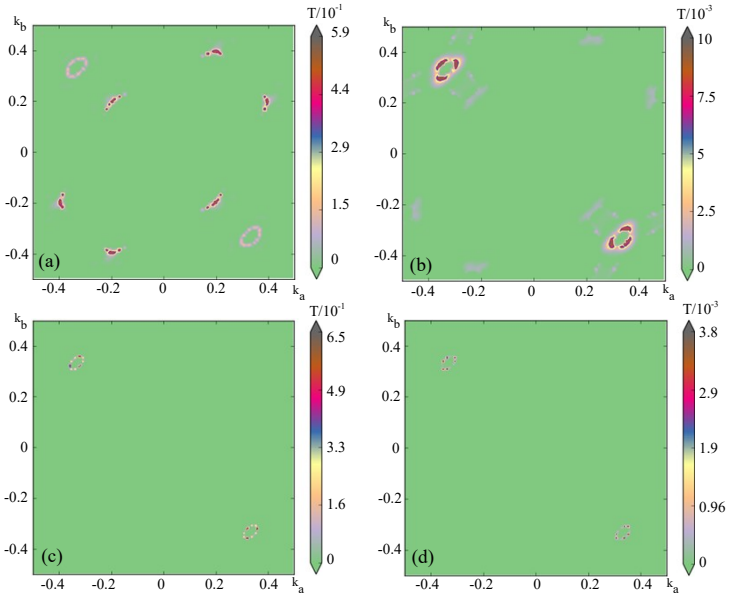

Fig. S14 Spin-denpendent transmission coefficients for 1H [(a) and (b)]and 3H devices [(c) and (d)] with SOC.[(a) and (c)] are for PC,[(b) and (d)] are for APC.

Table. S1 The interface barrier properties of 1H and 3H heterostructures, including the tunneling barrier height (Φ_{TB}), width (W_{TB}) and probability (P_{TB}).

Barrier	B1	B2	B3	B4	B5
Φ_{TB}(eV)	0.48	6.49	6.65	5.55	6.52
W_{TB}(Å)	0.35	1.34	1.34	1.18	1.37
P_{TB}(%)	77.98	3.01	2.87	5.81	2.74

Table. S2 Spin-dependent conductance and TMRs of 1H devices under different Hubbard-U.

Hubbard-U	$G_{PC}^{\uparrow\uparrow}(\Omega)$	$G_{PC}^{\downarrow\downarrow}(\Omega)$	$P_{PC}(\%)$	$G_{APC}^{\uparrow\uparrow}(\Omega)$	TMR(%)
0eV	2.11×10^{-8}	9.09×10^{-8}	62.32	1.63×10^{-9}	3.35×10^{3}
2.0eV	5.03×10^{-9}	2.00×10^{-9}	43.10	3.67×10^{-9}	-4.25
2.32eV	5.00×10^{-8}	1.59×10^{-9}	93.84	3.35×10^{-9}	0.67×10^{3}
3.0eV	4.02×10^{-9}	1.37×10^{-9}	49.17	1.17×10^{-9}	0.13×10^{3}

Table. S3 Spin-dependent conductance and TMRs of 3H devices under different Hubbard-U.

Device structure	$G_{PC}^{\uparrow\uparrow}(\Omega)$	$G_{PC}^{\downarrow\downarrow}(\Omega)$	$P_{PC}(\%)$	$G_{APC}^{\uparrow\uparrow}(\Omega)$	TMR(%)
0eV	1.10×10^{-8}	2.38×10^{-12}	99.95	2.88×10^{-11}	1.83×10^{4}
2.0eV	4.52×10^{-9}	1.17×10^{-12}	99.95	0.53×10^{-9}	0.32×10^{3}
2.32eV	4.67×10^{-9}	1.04×10^{-12}	99.96	0.65×10^{-10}	3.50×10^{3}
3.0eV	1.45×10^{-9}	7.81×10^{-13}	99.89	0.60×10^{-11}	1.20×10^{4}

Table. S4 Spin-dependent conductance and TMRs of two types of devices including using advanced pseudopotential.

Device structure	$G_{PC}^{\uparrow\uparrow}(\Omega^{-1})$	$G_{PC}^{\downarrow\downarrow}(\Omega^{-1})$	$P_{PC}(\%)$	$G_{APC}^{\uparrow\uparrow}(\Omega^{-1})$	TMR(%)
1H	3.62×10^{-8}	5.22×10^{-8}	18.10	1.00×10^{-10}	4.39×10^{4}
3H	3.44×10^{-9}	6.54×10^{-13}	99.96	1.23×10^{-13}	1.40×10^{6}